

Thickness dependence of linearly polarized light-induced momentum anisotropy and inverse spin Hall effect in topological insulator Bi_2Te_3

Jiayi Qiu(邱嘉毅), Jinling Yu(俞金玲), Zhu Diao(刁佇), Yunfeng Lai(赖云锋), Shuying Cheng(程树英), Yonghai Chen(陈涌海), and Ke He(何珂)

Citation: Chin. Phys. B, 2025, 34 (**11**): 117103. DOI: 10.1088/1674-1056/adf82a
http://cpb.iphy.ac.cn; http://iopscience.iop.org/cpb

What follows is a list of articles you may be interested in

Effect of lattice distortion on spin admixture and quantum transport in organic devices with spin-orbit coupling

Ying Wang(王莹), Dan Li(李丹), Xinying Sun(孙新英), Huiqing Zhang(张惠晴), Han Ma(马晗), Huixin Li(李慧欣), Junfeng Ren(任俊峰), Chuankui Wang(王传奎), and Guichao Hu(胡贵超)

Chin. Phys. B, 2024, 33 (**7**): 077101. DOI: 10.1088/1674-1056/ad35ae

Investigation of helicity-dependent photocurrent of surface states in $(Bi_{0.7}Sb_{0.3})_2Te_3$ nanoplate

Qin Yu(喻钦), Jinling Yu(俞金玲), Yonghai Chen(陈涌海), Yunfeng Lai(赖云锋), Shuying Cheng(程树英), and Ke He(何珂)

Chin. Phys. B, 2024, 33 (**5**): 057101. DOI: 10.1088/1674-1056/ad322c

Helicity-dependent photoconductance of the edge states in the topological insulator Bi_2Te_3

Yuchao Zhou(周宇超), Jinling Yu(俞金玲), Yonghai Chen(陈涌海), Yunfeng Lai(赖云锋), and Shuying Cheng(程树英)

Chin. Phys. B, 2023, 32 (**8**): 087102. DOI: 10.1088/1674-1056/acc3fb

Structural, electronic, optical, and magnetic properties of Co-doped Cu_2O

I Djabri, T Rezkallah, F Chemam

Chin. Phys. B, 2017, 26 (**2**): 027102. DOI: 10.1088/1674-1056/26/2/027102

Thickness dependence of the anomalous Hall effect in disordered face-centered cubic FePt alloy films

Chen Ming (陈明), He Pan (何攀), Zhou Shi-Ming (周仕明), Shi Zhong (时钟)

Chin. Phys. B, 2014, 23 (**1**): 017104. DOI: 10.1088/1674-1056/23/1/017104

RAPID COMMUNICATION

Thickness dependence of linearly polarized light-induced momentum anisotropy and inverse spin Hall effect in topological insulator Bi_2Te_3

Jiayi Qiu(邱嘉毅)[1,2], Jinling Yu(俞金玲)[1,†], Zhu Diao(刁佇)[2], Yunfeng Lai(赖云锋)[1], Shuying Cheng(程树英)[1], Yonghai Chen(陈涌海)[3], and Ke He(何珂)[4]

[1] *Institute of Micro/Nano Devices and Solar Cells, School of Physics and Information Engineering, Fuzhou University, Fuzhou* 350108, *China*
[2] *Department of Electronic Engineering and Maynooth International Engineering College, Maynooth, Co. Kildare, Ireland*
[3] *Laboratory of Solid State Optoelectronics Information Technology, Institute of Semiconductors, Chinese Academy of Sciences, Beijing* 100083, *China*
[4] *Department of Physics, State Key Laboratory of Low Dimensional Quantum Physics, Tsinghua University, Beijing* 100084, *China*

(Received 2 June 2025; revised manuscript received 18 July 2025; accepted manuscript online 6 August 2025)

The thickness dependence of linearly polarized light-induced momentum anisotropy and the inverse spin Hall effect (PISHE) in topological insulator (TI) Bi_2Te_3 films has been investigated. A significant enhancement of the PISHE signal is observed in the 12-quintuple-layer (QL) Bi_2Te_3 film compared with that of the 3- and 5-QL samples, whereas a minimal value of photoinduced momentum anisotropy is found in the 12-QL sample. The photoinduced momentum anisotropy and the PISHE in Bi_2Te_3 films are more than three and two orders of magnitude larger than those in Bi_2Se_3 films grown on $SrTiO_3$ substrates, respectively. The 3-QL sample exhibits a sinusoidal dependence of the PISHE current on the light spot position, while the 5-QL and 12-QL samples show a W-shaped dependence, which arises from the different angles between the coordinate axis x and the in-plane crystallographic axis of the Bi_2Te_3 films. Our findings demonstrate the critical role of film thickness in modulating both the photoinduced momentum anisotropy and the PISHE current, thereby suggesting a thickness-engineering strategy for designing novel optoelectronic devices based on TIs.

Keywords: photoinduced inverse spin Hall effect, photoinduced momentum anisotropy, three-dimensional topological insulator, Bi_2Te_3, thickness dependence

PACS: 71.70.Ej, 72.25.Fe, 75.70.Tj, 75.76.+j

DOI: 10.1088/1674-1056/adf82a **CSTR:** 32038.14.CPB.adf82a

1. Introduction

Three-dimensional (3D) topological insulators (TIs) have shown great potential in advancing spintronics, optoelectronics, and quantum computing, owing to their unique spin–momentum-locked surface states and strong spin–orbit coupling (SOC).[1–4] The photoinduced inverse spin Hall effect (PISHE), which converts spin current into charge current, provides an electrical means to detect spin current.[5–11] Notably, the PISHE offers a powerful approach to investigate the inverse spin Hall effect (ISHE) of topological insulators at room temperature without external magnetic fields.[12]

TIs such as Bi_2Se_3, Sb_2Te_3, and Bi_2Te_3 are considered ideal spintronic materials due to their spin–momentum-locked Dirac surface states. Bi_2Te_3 is a model 3D TI owing to its single Dirac point with linear Dirac-type electronic bands, strong SOC, and helical spin–momentum locking in the surface states.[13–15] Previous studies have investigated the PISHE induced by circularly polarized light in three-dimensional TIs such as Bi_2Se_3, Sb_2Te_3, and Bi_2Te_3, as well as the PISHE induced by linearly polarized light in Bi_2Se_3.[12,16–18] Moreover, momentum anisotropy induced by linearly polarized light has been observed in AlGaN/GaN heterostructures and in 3D TI Bi_2Se_3 films grown on $SrTiO_3$ substrates via the anomalous linear photogalvanic effect (ALPGE).[12,19] However, the thickness dependence of the PISHE and the momentum anisotropy induced by linearly polarized light remains unexplored.

In this paper, the thickness dependence of photoinduced momentum anisotropy and PISHE in 3D TI Bi_2Te_3 induced by linearly polarized light is systematically investigated. It is found that the 12-quintuple-layer (QL) Bi_2Te_3 film exhibits a maximum PISHE signal and a minimal photoinduced momentum anisotropy compared with the 3-QL and 5-QL samples. Furthermore, the photoinduced momentum anisotropy and the PISHE current in Bi_2Te_3 films are more than three and two orders of magnitude larger than those in Bi_2Se_3 films grown on $SrTiO_3$ substrates, respectively. This phenomenon may be attributed to the higher light absorption coefficient of Bi_2Te_3 films and the photo-generated carrier injection effect from the Si substrate. The spatial distribution of the PISHE current also varies with film thickness: the 3-QL sample exhibits a sinusoidal dependence of PISHE current on the light spot position, whereas the 5-QL and 12-QL samples show a W-shaped dependence. This behavior arises from the different angles be-

[†]Corresponding author. E-mail: jlyu@semi.ac.cn

© 2025 Chinese Physical Society and IOP Publishing Ltd. All rights, including for text and data mining, AI training, and similar technologies, are reserved.

tween the coordinate axis x and the in-plane crystallographic axis of Bi_2Te_3 films, as confirmed by fitting the light spot position dependence of the PISHE current to the theoretical model.

2. Experimental details

Bi_2Te_3 thin films with thicknesses of 3 QLs, 5 QLs, and 12 QLs were grown on insulating Si (111) substrates using the molecular beam epitaxy (MBE) method in an ultra-high vacuum chamber at a base pressure of 1×10^{-11} Pa. A pair of Ti/Au electrodes with a radius of 0.3 mm and a spacing of approximately 1.5 mm were deposited on the Bi_2Te_3 surface through electron beam evaporation. The samples were mounted in an optical cryostat at 290 K, equipped with a 1 Pa low-pressure chamber to prevent sample degradation.

A diode-pumped solid-state laser with a wavelength of 1064 nm and a power of 50 mW was used as the radiation source. After passing through a chopper, a polarizer, and a half-wave plate, the laser beam was normally incident on the sample, forming a light spot with a diameter of 0.5 mm. The light spot profile exhibited a Gaussian shape, which was characterized using a pyroelectric camera. The signal was extracted using a preamplifier and a lock-in amplifier synchronized with the chopper at a frequency of 229 Hz. The geometric schematic of the measurement setup is illustrated in Fig. 1(a).

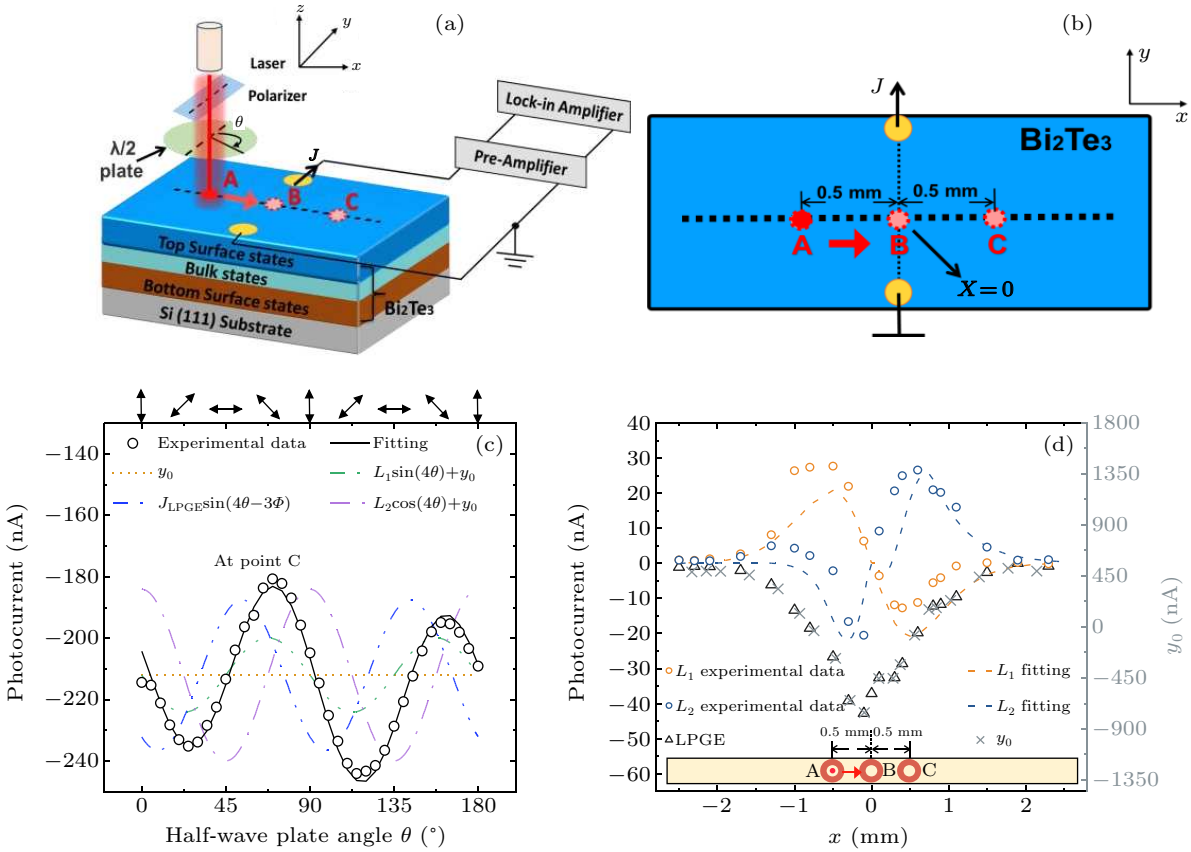


Fig. 1. (a) Schematic diagram of the photocurrent measurement geometry. (b) Illustration of the relationship between the photocurrent and the laser spot position. Points A, B, and C represent three specific positions along the perpendicular bisector of the line connecting the two electrodes. (c) Dependence of the photocurrent on the half-wave plate angle θ when the laser spot is normally incident at point C. (d) Spatial distributions of the LPGE, L_1, L_2, and y_0 in the 3-QL Bi_2Te_3 sample under normal incidence measured at 290 K. The symbols represent the experimental data, and the dashed lines are fitting curves obtained using Eqs. (3) and (5), respectively.

3. Results and discussion

Photocurrent measurements on the Bi_2Te_3 samples were performed at a temperature of 290 K. The photocurrents induced by the anomalous linear photogalvanic effect (ALPGE) and the photoinduced inverse spin Hall effect (PISHE) were measured using the same method as described in Ref. [20]. The laser spot was moved along the perpendicular bisector of the line connecting the two electrodes, as illustrated in Fig. 1(b). The coordinates of these points were defined as $x_A = -0.5$ mm, $x_B = 0$ mm, and $x_C = 0.5$ mm, respectively. The origin of the coordinate system was set at the midpoint B between the two electrodes. The y-axis was oriented along the line connecting the electrodes, and the x-axis was perpendicular to this direction within the sample plane. When the laser spot was normally incident at the midpoint B between the two electrodes, only the LPGE current was present due to the C_{3v} symmetry of the surface states in the sample. There were no contributions from the ALPGE or the PISHE when the light spot was illuminated at point B.[21] Therefore, the correspond-

ing photocurrent at point B can be described as

$$J = J_{\mathrm{LPGE}} \sin(4\theta - 3\Phi) + y_0. \quad (1)$$

Here, J_{LPGE} denotes the LPGE current, and Φ is the angle between the x-axis and the in-plane crystallographic axis of Bi_2Te_3. θ represents the angle between the polarization direction of the incident light and the optical axis of the half-wave plate. y_0 is the polarization-independent photocurrent, which arises from the photovoltaic effect, thermoelectric effect, or Dember effect.[22]

By fitting Eq. (1) to the photocurrent measured when the light spot was located at the midpoint between the two electrodes, the values of J_{LPGE} and the angle Φ were extracted. The spatial distribution of the LPGE current was determined from the spatial profile of y_0, as shown in Fig. 1(d). After obtaining the spatial distribution curve of the LPGE current, the photocurrent at different light spot positions can be expressed as[20]

$$J = J_{\mathrm{LPGE}} \sin(4\theta - 3\Phi) + L_1 \sin(4\theta) + L_2 \cos(4\theta) + y_0. \quad (2)$$

Here, L_1 and L_2 represent the contributions from the ALPGE and PISHE currents, respectively. Figure 1(c) shows the variation of the photocurrent as a function of the half-wave plate angle when the laser spot was positioned at point C on a 3-QL Bi_2Te_3 sample. The blue, green, and purple dashed lines correspond to the LPGE, L_1, and L_2 currents, respectively. The dotted line indicates the polarization-independent photocurrent y_0. The solid line represents the fitting curve using Eq. (2), indicating excellent agreement between the experimental data and the theoretical model.

By fitting the photocurrents measured at different laser spot positions with Eq. (2), the spatial distribution profiles of L_1 and L_2 were obtained, as shown in Fig. 1(d). Both L_1 and L_2 exhibited a sinusoidal dependence on the light spot position. The L_1 current is induced by the inhomogeneous light intensity distribution and the light momentum alignment effect.[19] The sinusoidal dependence of L_1 on the light spot position is consistent with previous observations reported in Refs. [19,20]. However, the sinusoidal dependence of L_2 on the spot position differs from that reported in Ref. [20], which exhibited a W-shaped dependence on the light spot position x. This difference arises from the distinct angles between the coordinate axis x and the in-plane crystallographic axis of Bi_2Te_3, compared with Bi_2Se_3 as reported in Ref. [20], as discussed below.

Figures 2(a)–2(c) show the dependence of the LPGE, L_1, and L_2 currents on the half-wave plate angle θ for the 3-QL sample when the laser spot was illuminated at points A, B, and C, respectively. It can be observed that as the laser spot traversed the perpendicular bisector between the two electrodes, the LPGE current maintained a constant phase, whereas both L_1 and L_2 currents exhibited a 180° phase shift. When the laser spot was located at the midpoint between the two electrodes, both L_1 and L_2 currents were zero.

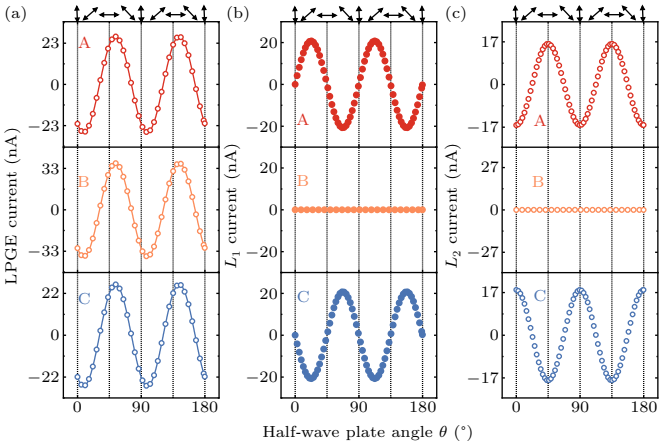


Fig. 2. (a)–(c) LPGE, L_1, and L_2 currents as a function of the half-wave plate angle θ at points A, B, and C, respectively, obtained by fitting the experimental data using the theoretical models described in Eqs. (3) and (5) for the 3-QL sample.

4. Determination of photoinduced momentum anisotropy

Figures 3(a)–3(c) display the spatial dependence of the L_1 current in the Bi_2Te_3 thin films with thicknesses of 3 QLs, 5 QLs, and 12 QLs, respectively. In all three samples, the L_1 current exhibits a sinusoidal dependence on the light spot position. The L_1 current originates from the optical momentum alignment effect, which does not require the absence of inversion symmetry.[19] Therefore, both the topological surface states (SSs) and the bulk states contribute to the L_1 current. However, owing to the substantially higher electron mobility in the SSs compared with that in the bulk states, the L_1 current is predominantly generated by the SSs.

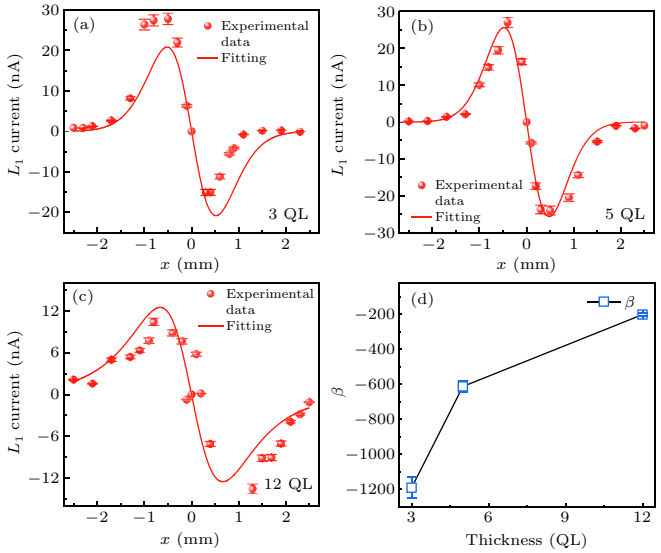


Fig. 3. (a)–(c) Dependence of the L_1 current on the light spot position x in Bi_2Te_3 films with thicknesses of 3 QLs, 5 QLs, and 12 QLs, measured at 290 K. The solid circles represent the experimental data, and the solid lines are the fitting results using Eq. (3). (d) Dependence of the photoinduced momentum anisotropy β on the film thickness.

5. Determination of photoinduced momentum anisotropy

Accounting for the Gaussian profile of the light spot, the spatial distribution of the L_1 current can be represented as[19]

$$L_1 = \frac{4WP_{xy}}{\pi\sigma R}\frac{xL}{(x^2+L^2)^2}\exp\left(-x^2/A_s\right), \tag{3}$$

where W is the incident light power and R denotes the resistance between the two electrodes. x represents the laser spot position, and σ is the conductivity. L is half of the distance between the electrodes, and $\exp(-x^2/A_s)$ is a Gaussian decay factor describing the spatial intensity distribution of the laser spot. P represents the ALPGE tensor, whose off-diagonal element is given by

$$P_{xy} = \alpha\beta(\theta)\frac{2e(\upsilon_e\tau)^2}{\hbar\omega}. \tag{4}$$

Here, α is the absorption coefficient, and υ_e denotes the electron velocity near the Fermi level. $\hbar\omega$ is the photon energy of the excitation light, and τ is the relaxation time, including contributions from momentum and energy relaxation as well as the carrier lifetime. β is the momentum anisotropy factor, defined as $\beta(\theta) = \int g(\theta,\theta_0)\sin\theta\cos\theta\,\mathrm{d}\theta$, where $g(\theta,\theta_0)$ describes the conditional probability for photoexcited carriers to acquire momentum orientation θ under linearly polarized light with polarization angle θ_0. The term $\sin\theta\cos\theta$ acts as a projection factor quantifying the net asymmetry contributing to the transverse photocurrent perpendicular to the incident light.

The photoinduced momentum anisotropy β is an essential quantity for quantifying the optical momentum alignment effect, which contributes to the L_1 current. To determine β, Eq. (3) is first used to fit the experimental data, yielding the factor $4WP_{xy}/(\pi\sigma R)$. The resulting fitting curves, shown as solid lines in Figs. 3(a)–3(c), exhibit excellent agreement with the experimental results. Using the obtained fitting parameter and the following known quantities, β can be calculated. The electron velocity υ_e is 8.77×10^5 m/s, as determined by angle-resolved photoemission spectroscopy (ARPES),[20] and the light power W is 50 mW from experiment. For the 3-QL, 5-QL, and 12-QL samples, the conductivities σ are 6.00×10^{-5} S/m, 1.11×10^{-4} S/m, and 5.57×10^{-5} S/m, respectively, based on previous work.[23] The absorption coefficients α are estimated as 0.011, 0.018, and 0.043 for the corresponding film thicknesses.[24]

Given that the circular photogalvanic effect (CPGE) current depends linearly on the momentum relaxation time, the thickness-dependent momentum relaxation time in Bi_2Te_3 films can be estimated by comparing the CPGE current amplitudes across different thicknesses under identical optical conditions. The CPGE currents for the 3-QL, 5-QL, and 12-QL Bi_2Te_3 films are 23 nA, 25 nA, and 10 nA, respectively, under 1064 nm, 50 mW illumination at a 30° incident angle (see Fig. 6). Considering the typical value $\tau_p = 0.25$ ps for Bi_2Te_3 thin films,[20] the momentum relaxation times for the 3-QL, 5-QL, and 12-QL films are estimated as 0.25 ps, 0.27 ps, and 0.11 ps, respectively. Consequently, the photoinduced momentum anisotropy β is calculated to be −1192.4, −612.6, and −200.8 for the 3-QL, 5-QL, and 12-QL Bi_2Te_3 thin films, respectively, as shown in Fig. 3(d).

It is evident that the photoinduced momentum anisotropy β in Bi_2Te_3 thin films grown on Si substrates is over three orders of magnitude larger than that in Bi_2Se_3 films grown on $SrTiO_3$ substrates.[20] This demonstrates that Bi_2Te_3 exhibits an excellent response to linearly polarized light, showing great potential for applications in linear polarization detection. The remarkable enhancement is attributed to the larger optical absorption coefficient of Bi_2Te_3 and the photoinduced carrier injection from the Si substrate, as evidenced by the much greater y_0 in Bi_2Te_3 compared with Bi_2Se_3.[12]

As the thickness of the Bi_2Te_3 film increases from 3 QL to 12 QL, the extracted β value decreases significantly. This observation reveals a strong dependence of the photoinduced momentum anisotropy on film thickness, which may be attributed to two main factors. Firstly, according to Ref. [25], the Fermi level shifts toward the bulk bandgap of Bi_2Te_3 as the film thickness increases. Consequently, the photoexcited carriers in thicker films possess smaller average momentum, leading to a reduction in the L_1 current. Secondly, with increasing film thickness, the hybridization between the top and bottom surface states becomes weaker,[25] which further contributes to the suppression of the L_1 current.

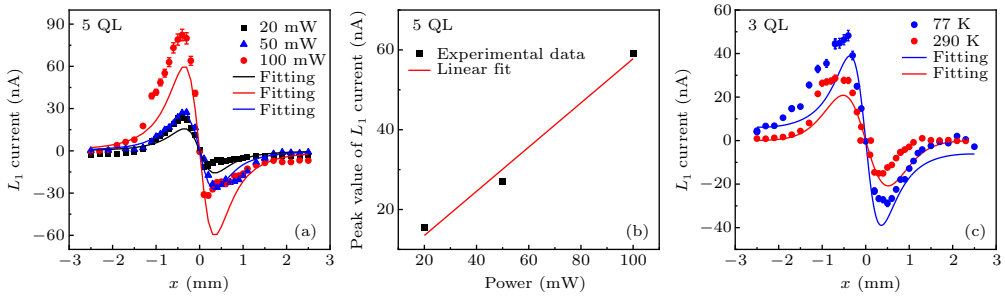


Fig. 4. (a) Dependence of the L_1 current on the light spot position x for the 5-QL Bi_2Te_3 film under 1064 nm excitation at different light powers, measured at 290 K. The solid lines represent the fitting curves using Eq. (3). (b) Dependence of the peak L_1 current values obtained from the fits in panel (a) on the excitation light power. (c) Dependence of the L_1 current on the light spot position x for the 3-QL Bi_2Te_3 film measured at 77 and 290 K.

Figure 4(a) shows the dependence of the L_1 current on the light spot position x for the 5-QL Bi_2Te_3 film under 1064 nm excitation with different optical powers, where the solid lines represent the fitting curves obtained using Eq. (3). Figure 4(b) displays the dependence of the peak values of the L_1 current (from the fits) on the incident light power, with the solid line showing a linear fit. It is clear that the L_1 current increases nearly linearly with increasing light power. Figure 4(c) presents the L_1 current as a function of the light spot position x for the 3-QL Bi_2Te_3 film measured at 77 K and 290 K, respectively. It can be seen that the L_1 current increases as the temperature decreases. This enhancement can be attributed to the increase in the momentum relaxation time τ_p at lower temperatures.

5.1. PISHE induced by linearly polarized light

Figures 5(a)–5(c) show the spatial dependence of the L_2 current for Bi_2Te_3 thin films with thicknesses of 3 QLs, 5 QLs, and 12 QLs, respectively. In the 3 QL sample, the L_2 current exhibits a sinusoidal dependence on light spot positions, whereas in the 5 QL and 12 QL samples, the L_2 current shows a W-shaped dependence on light spot positions.

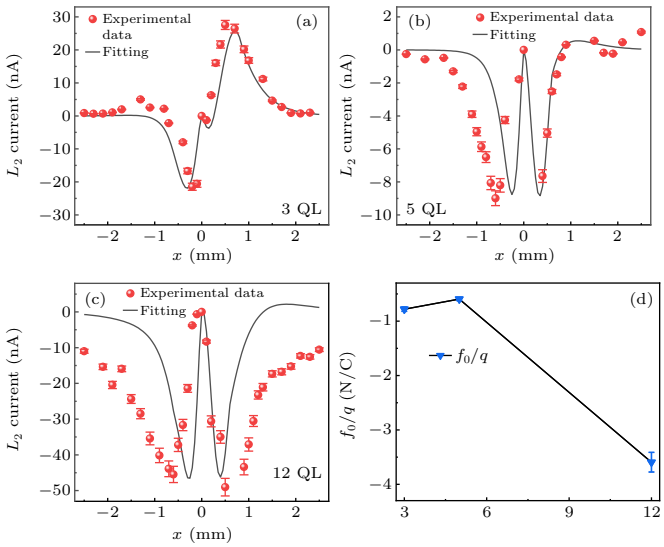


Fig. 5. (a)–(c) Dependence of the L_2 current on the light spot position for Bi_2Te_3 films with different thicknesses. Solid circles represent experimental data, and solid lines are fitting results using Eq. (5). (d) Thickness dependence of the spin transverse force f_0/q for the 3-QL, 5-QL, and 12-QL samples.

The L_2 component is proportional to the strength of the SOC and is primarily contributed by the SSs.[20] Specifically, under linearly polarized light illumination, electrons are excited from below the Fermi level to higher-energy states. According to optical transition selection rules, linearly polarized light generates photoexcited carriers in the states $|\boldsymbol{k},\uparrow\rangle$ and $|-\boldsymbol{k},\downarrow\rangle$. Although these carriers possess opposite momenta and do not contribute to a net charge current, their opposite spin polarizations produce a net spin current. Under the inverse spin Hall effect (ISHE), this spin current experiences a transverse spin force f_0, leading to a measurable photocurrent, which corresponds to the L_2 current. This photocurrent is collected by the two electrodes and can be described by[20]

$$I_{ab} = \frac{f_0}{\sqrt{2\pi}q\chi}\iint_D \exp\left(-\frac{r^2}{2\chi^2}\right)\cos\left(3\left(\varphi-\Theta\right)\right) \times\left(\cos 2\varphi + I_1\right) r\,\mathrm{d}r\,\mathrm{d}\varphi. \tag{5}$$

Here, q is the electron charge, and D denotes the triangular area defined by the center of the laser spot and the two electrodes. f_0 represents the transverse spin force, and I_1 is a constant.

According to Ref. [26], spatially localized topological SSs in the sample give rise to a pronounced hexagonal warping effect, resulting in a significant out-of-plane spin component (OPSC) characterized by a $\cos(3\varphi-\pi/2)$ dependence. Here, φ denotes the azimuthal angle measured counterclockwise from the Γ–M direction, where Γ is the zone center and M is the midpoint of a hexagonal Brillouin zone edge of Bi_2Te_3. Considering that the x-axis and the in-plane crystallographic axis of Bi_2Te_3 form an angle Φ, the OPSC induced by hexagonal warping can be written as $\cos(3\varphi-\pi/2-3\Phi)$. Denoting $\Theta=\pi/6+\Phi$, the OPSC can be expressed as $\cos(3(\varphi-\Theta))$, as used in Eq. (5). Therefore, Θ reflects the angle between the x-axis and the in-plane crystallographic axis of Bi_2Te_3.

It can be seen from Figs. 5(a)–5(c) that the spatial distribution of the L_2 current for the 3-QL sample differs from those of the 5-QL and 12-QL samples. This difference may be related to variations in the angle Θ for samples with different thicknesses. To investigate the influence of Θ, we simulated the spatial distribution of the L_2 current for different Θ values, as shown in Fig. 6(c). Evidently, varying Θ leads to distinct shapes of the L_2 current spatial profiles.

We then fitted Eq. (5) to the experimental data in Fig. 5. For the 3-QL sample, the best fit is obtained with $\Theta=15°$, where the L_2 current exhibits an antisymmetric sinusoidal dependence on the light spot position. In contrast, for the 5-QL and 12-QL samples, the optimal fit occurs at $\Theta=-19.5°$, with the L_2 current showing a symmetric W-shaped dependence. This distinct behavior highlights that the difference between the 3-QL sample and the thicker 5-QL or 12-QL samples arises from Θ-angle variations correlated with film thickness. For thicker samples, Θ appears to converge to approximately $-19.5°$, but this inference requires further experimental verification. The angle Θ is closely related to the growth conditions, particularly the substrate properties. The detailed mechanisms underlying these effects remain unclear and warrant further theoretical and experimental investigation.

The L_2 current is induced by normally incident linearly polarized light and represents the superposition of the PISHE currents from the top and bottom surface states of the Bi_2Te_3 film. To analyze the thickness dependence of the PISHE currents, it is essential to determine whether the observed PISHE

current originates predominantly from the top or bottom surface states. Considering that the circular photogalvanic effect (CPGE) is also proportional to the SOC strength of the surface states, similar to the PISHE, we measured the CPGE current under both front and back illuminations for all samples, following the method reported in Ref. [18].

Figure 7(a) shows a schematic of the setup for CPGE measurement, using a diode-pumped solid-state laser with a wavelength of 1064 nm as the radiation source. A polarizer and a quarter-wave plate generate circularly polarized light. The laser beam is incident at the midpoint of the interelectrode gap with a spot diameter of approximately 500 μm and an incident angle Υ. Figure 7(a) also illustrates the experimental geometries for CPGE measurements under front and back illuminations. The CPGE current is extracted by fitting the polarization state-dependent photocurrent I with the following equation:[18]

$$I = I_{\mathrm{CPGE}}\sin(2\theta_0) + I_{\mathrm{LPGE1}}\sin(4\theta_0) + I_{\mathrm{LPGE2}}\cos(4\theta_0) + I_0. \tag{6}$$

Here, I_{CPGE} is the CPGE current induced by circularly polarized light, and I_0 is the polarization-independent photocurrent. I_{LPGE1} and I_{LPGE2} are the LPGE currents arising from linearly polarized light excitation. The CPGE current can be phenomenologically expressed as

$$I_{\mathrm{CPGE}} = \gamma P_{\mathrm{circ}}|E_0|^2 t_{\mathrm{p}} t_{\mathrm{s}} \sin\Upsilon',$$

where γ and E_0 are the material-symmetry-related tensor and electric field amplitude of the light, respectively. t_{p} and t_{s} are the transmission coefficients for p- and s-polarized light, respectively. $P_{\mathrm{circ}} = (I_{\sigma+} - I_{\sigma-})/(I_{\sigma+} + I_{\sigma-})$ is the light helicity. The refraction angle Υ' satisfies $\sin\Upsilon' = \sin\Upsilon/n$, where n is the refractive index of the material.

Figures 7(b)–7(d) show the dependence of the CPGE current on the incident angle under front and back illuminations for 3-, 5-, and 12-QL Bi_2Te_3 films, respectively. For the 3-QL sample, the CPGE current exhibits opposite signs under front and back illuminations, indicating that it originates primarily from the top surface states under front illumination, with the dominant contribution switching to the bottom surface states under back illumination.[18] In contrast, for the 5-QL and 12-QL samples, the CPGE current exhibits the same sign under both front and back illuminations, indicating that the current is dominated by the same surface states in both cases. Given that the CPGE of the 5-QL and 12-QL samples under front illumination shows the same incident-angle dependence as the 3-QL sample, it can be inferred that the CPGE current is mainly contributed by the top surface states for all samples. Since the PISHE depends similarly on the spin–momentum locking mechanism of the topological surface states, we can conclude that the L_2 current is dominated by the top surface states under front illumination for the 3-QL, 5-QL, and 12-QL Bi_2Te_3 films.

By fitting the experimentally measured L_2 current with Eq. (5), the spin transverse force f_0/q experienced by electrons in the samples can be extracted, yielding values of -0.7812 N/C, -0.5937 N/C, and -3.5937 N/C for the 3-QL, 5-QL, and 12-QL samples, respectively. The fitting results are shown by solid lines in Figs. 5(a)–5(c), and the extracted values of f_0/q are summarized in Fig. 5(d).

As shown in Fig. 5, with increasing film thickness from 3 QL to 12 QL, the peak value of the PISHE (i.e., L_2) current first decreases and then increases. Different values of Θ contribute to variations in the peak PISHE current, as illustrated in Fig. 6(c). To eliminate the influence of Θ, we fit the experimental data using Eq. (5) and obtained the spin transverse force f_0/q shown in Fig. 5(d). It is evident that as the Bi_2Te_3 film thickness increases from 3 QL to 12 QL, the spin transverse force f_0/q decreases. This behavior may be attributed to two main factors.

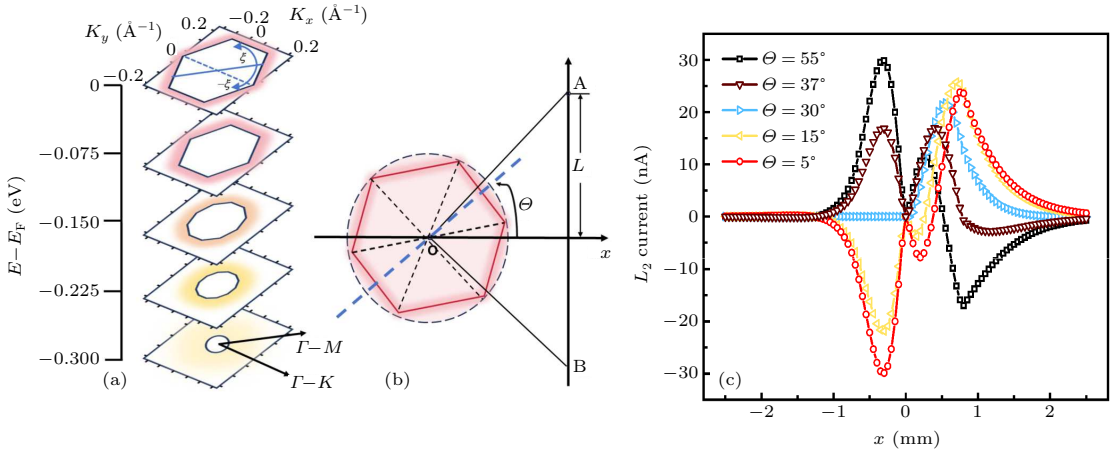


Fig. 6. (a) Schematic illustration of hexagonal warping in the electronic states based on ARPES measurements.[25] This indicates a strong out-of-plane spin polarization near the Fermi level, which decreases with increasing binding energy. The blue dashed line connecting the hexagon vertex (K point) to its zone center (Γ point) represents the Γ–K direction, while the blue solid line connecting the side center point (M point) to the center corresponds to the Γ–M direction. (b) Schematic diagram of the laser spot and electrode configuration. Dashed circles indicate the light spot, and dots A and B denote the two electrodes. (c) Calculated spatial distributions of the L_2 current for different Θ values.

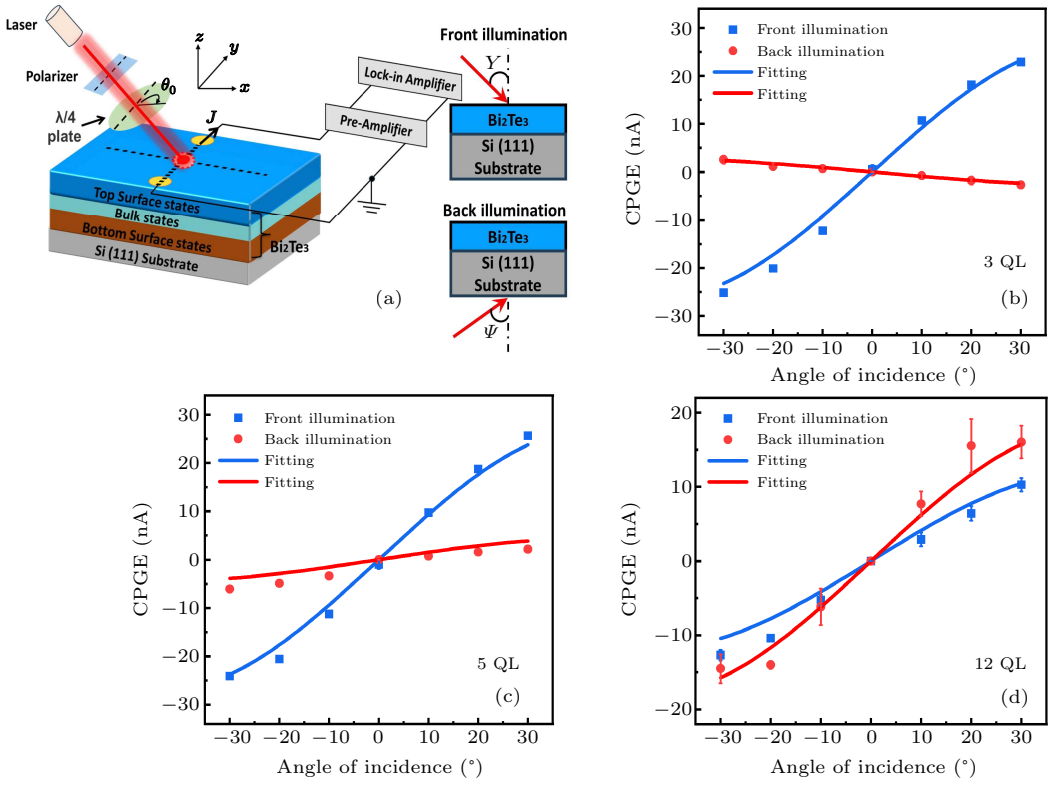


Fig. 7. (a) Experimental setup for CPGE measurements under front and back illumination for Bi_2Te_3 films grown on Si (111) substrates. (b)–(d) Dependence of the CPGE current on the incident angle for 3-QL, 5-QL, and 12-QL Bi_2Te_3 samples under front and back illumination with 1064 nm light at 50 mW.

Firstly, as the film thickness increases, the light intensity reaching the bottom surface is attenuated, reducing the spin transverse force experienced by the bottom surface states. Since the spin transverse forces of the top and bottom surface states have opposite signs, they partially cancel each other.[16] Because the net spin transverse force is dominated by the top surface states, the reduction in the bottom surface contribution enhances the net spin transverse force. For the 3-QL and 5-QL samples, the thickness is small, resulting in minimal light intensity difference between the top and bottom surfaces, and hence a small net spin transverse force. In contrast, the 12-QL sample has a greater thickness, producing a larger disparity in light intensity between the top and bottom surfaces and a correspondingly enhanced net spin transverse force compared to the 3-QL and 5-QL samples.

Secondly, as the film thickness increases from 3 QLs to 12 QLs, the interface quality may change, which directly modulates the spin relaxation time of the topological surface states. Due to the linear proportionality between the spin relaxation time and the PISHE current, this effect further influences the magnitude of the observed L_2 current.

Figure 8(a) shows the dependence of the L_2 current on the light spot positions for the 5-QL Bi_2Te_3 film under 1064 nm excitation at different light powers. The solid lines represent the fitting curves using Eq. (5). From these fits, the spin transverse force f_0/q under varying excitation powers is extracted, as shown in Fig. 8(b). It is evident that the magnitude of f_0/q increases approximately linearly with light power.

Figure 8(c) presents the dependence of the L_2 current on the light spot positions for the 3-QL Bi_2Te_3 film measured at 77 K and 290 K. The L_2 current shows negligible temperature dependence, which may be attributed to the nearly temperature-independent spin relaxation time of the Dirac surface states.[27]

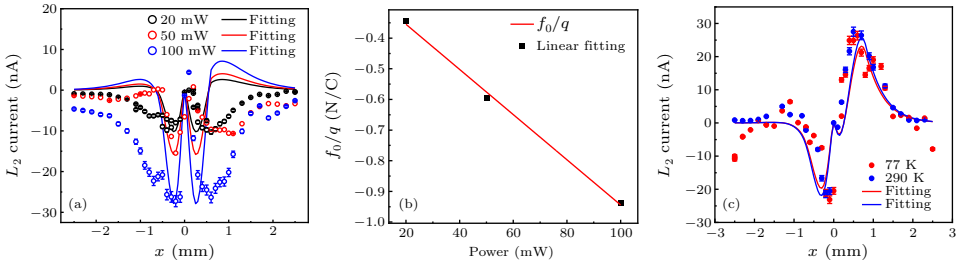


Fig. 8. (a) Dependence of the L_2 current on the light spot position x for the 5-QL Bi_2Te_3 film under 1064 nm excitation at different powers measured at 290 K. Solid lines represent the fitting curves using Eq. (5). (b) Dependence of the spin transverse force f_0/q obtained from fitting on the light power. (c) Dependence of the L_2 current on the light spot position x for the 3-QL Bi_2Te_3 film measured at 77 K and 290 K.

Notably, the PISHE current in the Bi_2Te_3 thin films grown on Si substrates is more than two orders of magnitude larger than that in the 7-QL Bi_2Se_3 film grown on $SrTiO_3$ substrates,[12] indicating that the Bi_2Te_3 films possess a very high spin-to-charge conversion efficiency and are promising for applications in data storage, magnetic sensors, communications, and biomedical devices. This significant enhancement can be primarily attributed to two factors. Firstly, the light absorption coefficient of Bi_2Te_3 grown on Si is considerably larger than that of Bi_2Se_3 grown on $SrTiO_3$, as evidenced by the much larger y_0 current observed in the Bi_2Te_3/Si sample ($\sim$ 900 nA) compared with the Bi_2Se_3/$SrTiO_3$ sample ($\sim$ 0.3 nA). Secondly, spin injection from the Si substrate further enhances the PISHE current. In our previous work,[23] we demonstrated that spin injection from the Si substrate under 1064 nm circularly polarized light excitation significantly enhances the CPGE current, which is dominated by the topological surface states of TIs. Since the PISHE and CPGE share a similar dependence on the SOC strength of the surface states, the PISHE current is likewise enhanced by spin injection from the Si substrate. In contrast, $SrTiO_3$ substrates cannot absorb 1064 nm light, and therefore no comparable spin injection occurs in the Bi_2Se_3/$SrTiO_3$ sample.

6. Conclusion

In summary, we have systematically investigated the thickness dependence of photoinduced momentum anisotropy and the PISHE induced by linearly polarized light in 3D TI Bi_2Te_3 films of 3 QLs, 5 QLs, and 12 QLs grown on Si (111) substrates. Our results reveal that the photoinduced momentum anisotropy and the PISHE current in Bi_2Te_3 films are more than three orders and two orders of magnitude larger, respectively, than those in Bi_2Se_3 films grown on $SrTiO_3$ substrates. This enhancement can be attributed to the higher light absorption coefficient of Bi_2Te_3 and the photo-generated carrier injection from the Si substrate. The photoinduced momentum anisotropy reaches a minimum in the 12-QL sample, while the PISHE current achieves a maximum in the same sample. Furthermore, we found that Bi_2Te_3 films of different thicknesses exhibit distinct light spot position dependences for the PISHE current, arising from variations in the angle between the x-axis and the in-plane crystallographic axis of the films. These findings indicate that film thickness is a critical parameter for tuning photoinduced momentum anisotropy and PISHE current, providing a thickness-engineering strategy for designing novel optoelectronic devices based on topological insulators.

Acknowledgments

This work was supported by the National Natural Science Foundation of China (Grant Nos. 62074036, 61674038, and 11574302), the Foreign Cooperation Project of Fujian Province, China (Grant No. 2023I0005), the Open Research Fund Program of the State Key Laboratory of Low Dimensional Quantum Physics (Grant No. KF202108), the National Key Research and Development Program of China (Grant No. 2016YFB0402303), and the Foundation of the Fujian Provincial Department of Industry and Information Technology of China (Grant No. 82318075).

References

[1] Xue H P, Sun R, Yang X, Liu J N, Yang Q L, Yang P T, Deng Z, Li X M, Bai X D, Zhang X Q, He W and Cheng Z H 2015 *Phys. Rev. B* **111** 075104
[2] Mukhopadhyay S, Pal P K, Manna S, Mitra C and Barman A 2015 *Phys. Rev. Appl.* **23** 014038
[3] Sun R, Sun Y B, Li N, Xue H P, Li Y, Yang X, Li Y, Comstock A H, Sun D L, Zhang X Q and Cheng Z H 2014 *Phys. Rev. B* **110** 024408
[4] Li J, Yin Z C, Li Q X and Zhu J J 2015 *Chin. Phys. B* **34** 037501
[5] Kumar N, Hait S, Pandey L, Sharma N, Gupta N K and Chaudhary S 2014 *Phys. Rev. B* **110** 134411
[6] Bader S D and Parkin S S P 2010 *Annu. Rev. Condens. Matter Phys.* **1** 71
[7] Hirsch J E 1999 *Phys. Rev. Lett.* **83** 1834
[8] Mosendz O, Pearson J E, Fradin F Y, Bauer G E, Bader S D and Hoffmann A 2010 *Phys. Rev. Lett.* **104** 046601
[9] Morota M, Niimi Y, Ohnishi K, Wei D H, Tanaka T, Kontani H, Kimura T and Otani Y 2011 *Phys. Rev. B* **83** 174405
[10] Hoffmann A 2013 *IEEE Trans. Magn.* **49** 5172
[11] Guo Q, Wu Y, Xu L, Gong Y, Ou Y, Liu Y, Li L, Yan Y, Han G, Wang D, Wang L, Long S, Zhang B, Cao X, Yang S, Wang X, Huang Y, Liu T, Yu G, He K and Teng J 2020 *Chin. Phys. Lett.* **37** 057301
[12] Yu J, Zeng X, Zhang L, He K, Cheng S, Lai Y, Huang W, Chen Y, Yin C and Xue Q 2017 *Nano Lett.* **17** 7878
[13] Chen Y L, Analytis J G, Chu J H, Liu Z K, Mo S K, Qi X L, Zhang H J, Lu D H, Dai X, Fang Z, Zhang S C, Fisher I R, Hussain Z and Shen Z X 2009 *Science* **325** 178
[14] Hsieh D, Xia Y, Qian D, Wray L, Meier F, Dil J H, Osterwalder J, Patthey L, Fedorov A V, Lin H, Bansil A, Grauer D, Hor Y S, Cava R J and Hasan M Z 2009 *Phys. Rev. Lett.* **103** 146401
[15] Xia Y, Qian D, Hsieh D, Wray L, Pal A, Lin H, Bansil A, Grauer D, Hor Y S, Cava R J and Hasan M Z 2009 *Nat. Phys.* **5** 398
[16] Wu W, Yu J, Jiang Y, Zeng X, Chen Y, Liu Y, Yin C, Cheng S, Lai Y, He K and Xue Q 2022 *Appl. Phys. Lett.* **120** 062407
[17] Wu W, Yu J, Xia L, Zhu K, Zeng X, Chen Y, Yin C, Cheng S, Lai Y and He K 2022 *Opt. Express* **30** 15085
[18] Yu J, Zhu K, Zeng X, Chen L, Chen Y, Liu Y, Yin C, Cheng S, Lai Y, Huang J, He K and Xue Q 2019 *Phys. Rev. B* **100** 235108
[19] Peng X Y, Zhang Q, Shen B, Shi J R, Yin C M, He X W, Xu F J, Wang X Q, Tang N, Jiang C Y, Chen Y H and Chang K 2011 *Phys. Rev. B* **84** 075341
[20] Yu J, Zeng X, Zhang L, Yin C, Chen Y, Liu Y, Cheng S, Lai Y, He K and Xue Q 2018 *Opt. Express* **26** 4832
[21] Olbrich P, Golub L E, Herrmann T, *et al.* 2014 *Phys. Rev. Lett.* **113** 096601
[22] McIver J W, Hsieh D, Steinberg H, Jarillo-Herrero P and Gedik N 2011 *Nat. Nanotechnol.* **7** 96
[23] Yu J, Xia L, Zhu K, Pan Q, Zeng X, Chen Y, Liu Y, Yin C, Cheng S, Lai Y, He K and Xue Q 2020 *ACS Appl. Mater. Interfaces* **12** 18091
[24] Ganeev R A, Popov V S, Zvyagin A I, Lavrentyev N A, Mirofyanchenko A E, Mirofyanchenko E V, Shuklov I A, Ovchinnikov O V, Ponomarenko V P and Razumov V F 2021 *Nanophotonics* **10** 3857
[25] Li Y Y, Wang G, Zhu X G, Liu M H, Ye C, Chen X, Wang Y Y, He K, Wang L L, Ma X C, Zhang H J, Dai X, Fang Z, Xie X C, Liu Y, Qi X L, Jia J F, Zhang S C and Xue Q K 2010 *Adv. Mater.* **22** 4002
[26] Bahramy M S, King P D C, Torre A D L, Chang J, Shi M, Patthey L, Balakrishnan G, Hofmann P, Arita R, Nagaosa N and Baumberger F 2012 *Nat. Commun.* **3** 1159
[27] Wang M C, Qiao S, Jiang Z, Luo S N and Qi J 2016 *Phys. Rev. Lett.* **116** 036601